

Multi-modal land cover mapping of remote sensing images using pyramid attention and gated fusion networks

Qinghui Liu^{a,b}, Michael Kampffmeyer^{b,a}, Robert Jenssen^{b,a} and Arnt-Børre Salberg^a

^aNorwegian Computing Center, Dept. SAMBA, P.O. Box 114 Blindern, NO-0314 Oslo, Norway; ^bUiT Machine Learning Group, Department of Physics and Technology, UiT the Arctic University of Norway, Tromsø, Norway

ARTICLE HISTORY

Compiled November 9, 2021

ABSTRACT

Multi-modality data is becoming readily available in remote sensing (RS) and can provide complementary information about the Earth’s surface. Effective fusion of multi-modal information is thus important for various applications in RS, but also very challenging due to large domain differences, noise, and redundancies. There is a lack of effective and scalable fusion techniques for bridging multiple modality encoders and fully exploiting complementary information. To this end, we propose a new multi-modality network (MultiModNet) for land cover mapping of multi-modal remote sensing data based on a novel pyramid attention fusion (PAF) module and a gated fusion unit (GFU). The PAF module is designed to efficiently obtain rich fine-grained contextual representations from each modality with a built-in cross-level and cross-view attention fusion mechanism, and the GFU module utilizes a novel gating mechanism for early merging of features, thereby diminishing hidden redundancies and noise. This enables supplementary modalities to effectively extract the most valuable and complementary information for late feature fusion. Extensive experiments on two representative RS benchmark datasets demonstrate the effectiveness, robustness, and superiority of the MultiModNet for multi-modal land cover classification.

KEYWORDS

Multiple modalities, Pyramid attention, Gated fusion, Multi-modal segmentation, Remote sensing

1. Introduction

Automatic mapping of land cover using remote sensing (RS) data is of great importance for a wide range of earth observation applications since it provides a fast and cost-effective solution for analyzing large areas (Salberg 2011; Audebert, Le Saux, and Lefèvre 2016). This includes applications like urban planning (Noor, Abdullah, and Hashim 2018), precision agriculture (Chiu et al. 2020a; Liu et al. 2020b), and disaster management (Salberg, Rudjord, and Solberg 2014; Bello and Aina 2014; Fan et al. 2021), to name a few. In the past few years, the emergence of deep learning and con-

CONTACT Qinghui Liu. Email: samleoqh@gmail.com

All the authors are associated with the Centre for Research-based Innovation *Visual Intelligence*: <http://visual-intelligence.no>, funded by the Research Council of Norway and consortium partners. RJ, MK and QL are with the UiT Machine Learning Group: <http://machine-learning.uit.no>.

volutional neural networks (CNNs) has led to significant improvements for land cover mapping in RS (Maggiori et al. 2017; Audebert, Le Saux, and Lefèvre 2018; Pashaei et al. 2020; Liu et al. 2020). Many existing deep learning approaches, however, only use unimodal remote sensing images, e.g., the standard three-channel data such as RGB or IRRG (NIR-Red-Green) images. Multi-modality data is becoming readily available and increasingly essential in remote sensing. This raises open challenges such as "what," "how," and "where" to effectively fuse multi-modal data (Hong et al. 2020) in order to develop joint representations of multiple modalities for enhancing land cover mapping performance.

Remote sensing imagery is often characterized by complex data properties in the form of heterogeneity and class imbalance, as well as overlapping class-conditional distributions that bring severe challenges for generating land cover maps or detecting and localizing objects, producing a high degree of uncertainty in obtained results. As shown in Fig. 1, mismapped or mislabeled results appear in the unimodal case for objects with similar color and texture, e.g., the roof of buildings vs. surfaces, and, the trees vs. low vegetation in Vaihingen dataset. On the other hand, our proposed multi-modal learning-based method alleviates these problems.

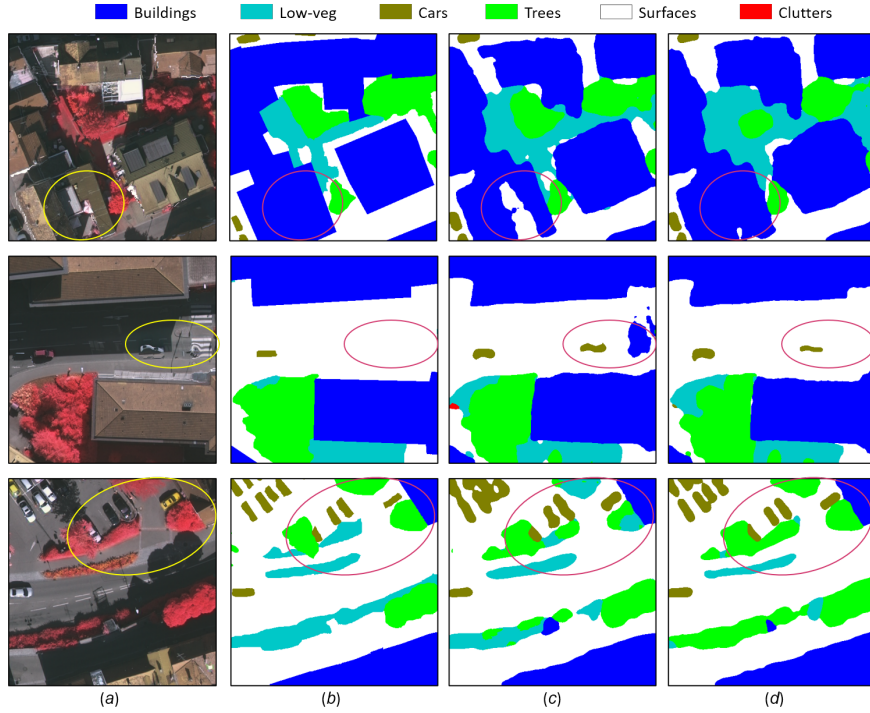


Figure 1. Mismapped or mislabeled examples in the Vaihingen dataset. (a) the IRRG images, (b) the labels, (c) the mapping results from a unimodal (only IRRG) model, and (d) the mapping results from our multi-modal (IRRG + DSM) model.

In order to improve the performance of semantic mapping that can be obtained from a single modality (e.g., RGB or IRRG), additional modalities, either from the same sensor (e.g. multi-spectral or hyperspectral images) or from a different one (e.g., LiDAR point cloud data or SAR) are increasingly used for land cover mapping (Hazirbas et al. 2016; Xu et al. 2017; Audebert, Le Saux, and Lefèvre 2018). Examples include Synthetic Aperture Radar (SAR) images (Hong et al. 2020; Li et al. 2020), hyperspectral imagery (HSI) (Xu et al. 2017; Audebert, Le Saux, and Lefèvre 2019) and Digital

Surface Models (DSM) (Hazirbas et al. 2016; Audebert, Le Saux, and Lefèvre 2018). Multi-modal data has been proven to provide rich complementary information to deal with complex scenes as different imaging technologies in RS are capable of capturing a variety of properties from the earth’s surface, such as height information, spectral radiance, and reflectance (Gómez-Chova et al. 2015).

One of the main challenges in the utilization of multi-modal data is how to effectively extract and fuse multi-modal features. Although deep learning-based methods can automatically learn representative features, multi-modal inputs and features often provide unequal, redundant, or even contradictory information. Current multi-modal models tend to extract features independently using two separate encoders, combining feature maps indiscriminately at early and/or late layers via concatenation or summation (Couprie et al. 2013; Audebert, Le Saux, and Lefèvre 2018). We argue that this design leads to both inaccurate and computationally inefficient models. In particular, it brings high sensitivity to missing or noisy data (Audebert, Le Saux, and Lefèvre 2018), which has a significant negative influence on overall model performance when dealing with missing or noisy modality scenarios (Kampffmeyer, Salberg, and Jenssen 2018). Another challenge of pixel-wise classification of multi-modal images is the increased model size and computational burden (Marmanis et al. 2016; Audebert, Le Saux, and Lefèvre 2018) that also limit the application in most scenarios with real-time requirements. Hence, the effective and efficient fusion of multi-modal information is still an open research direction and also needs to be further optimized for scalability and real-time consideration for real-world applications.

Recently, the usage of attention mechanisms and graph-based approaches has led to promising performance and computational efficiency gains on a range of different computer vision tasks (Mou and Zhu 2019; Fu et al. 2019; Liu et al. 2020b). These works, typically use these mechanisms to emphasize salient features and suppress irrelevant signals in unimodal settings. Further, they tend to ignore multi-scale information by only leveraging same-dimensional representations of the same scale (e.g., typically low-spatial-resolution feature spaces) in order to alleviate the computational cost. To facilitate an efficient multi-scale (pyramid) attention feature extraction from each modality, we propose a pyramid attention fusion (PAF) module for extracting multiple hierarchical-scale representations. By using a novel gated fusion unit (GFU) to blend complementary features between multi-modal encoders, we introduce a lightweight multi-modal segmentation network (MultiModNet). For more details, please refer to Section 3.

Our experiments demonstrate that the network achieves robust and accurate results on the representative ISPRS Semantic Labeling Contest Vaihingen dataset (Rottensteiner et al. 2012) and the Agriculture-Vision challenge dataset (Chiu et al. 2020b). The main contributions of this paper are as follows:

- (1) We present a novel pyramid attention and gated fusion mechanism for multi-modality data that builds on our proposed gated fusion unit (GFU) and our pyramid attention fusion (PAF) module. It facilitates interactions between the encoders of each modality to effectively combine the extracted features from multiple modalities and weaken the influence of noise and redundancies among the multi-modal data.
- (2) The proposed PAF module is a lightweight network with a built-in cross-hierarchical-scale and cross-view attention fusion mechanism that can obtain rich and robust contextual representations. It can be used as a stand-alone decoder for a unimodal model to improve segmentation performance, or as a vital

fusion mechanism to merge several modalities when combined with our gated fusion unit.

- (3) Built upon the PAF and GFU modules, our end-to-end multi-modal segmentation model (MultiModNet) achieves state-of-the-art performance and outperforms the baselines on two representative remote sensing datasets with considerably fewer parameters and at a lower computational cost. We also validate the effectiveness and flexibility of our framework through extensive ablation studies.

The paper is structured as follows. Section 2 provides an overview of the related work. In Section 3, we present the methodology in detail. Experimental procedure and evaluation of the proposed method is performed in Section 4. Section 5 further discusses and evaluates our method via ablation studies. Finally, we draw conclusions and outline future research directions in Section 6.

2. Related work

The state-of-the-art deep learning-based segmentation models are mostly inspired by the idea of fully convolutional networks (FCNs) (Long, Shelhamer, and Darrell 2015). FCN models generally consist of an encoder-decoder architecture in which all layers are based on convolutions (and upsampling/downsampling operations). However, vanilla FCNs tend to cause a loss of spatial information due to the presence of pooling layers that reduce the resolution of feature maps by sacrificing the positional information of objects. The UNet (Ronneberger, Fischer, and Brox 2015) extends the FCN by introducing symmetric skip connections (i.e., concatenations) between the encoder and decoder modules to maintain spatial information. The precise spatial information can be gradually recovered in the decoder module by combining multiple skipped connections with upsampling or de-convolution layers. Since then, the encoder-decoder architecture has been widely extended in recent works including, among others, pyramid scene parsing network (PSPNet) (Zhao et al. 2017), SegNet (Badrinarayanan, Kendall, and Cipolla 2017), DeepLabV3+ (Chen et al. 2018), Dual attention network (Fu et al. 2019), and HRNet-OCR (Yuan, Chen, and Wang 2020).

The FCN-based or UNet-based encoder-decoder architectures have also been widely adopted and applied to the ISPRS Semantic Labeling Contest (Paisitkriangkrai et al. 2015; Kampffmeyer, Salberg, and Jenssen 2016; Sherrah 2016; Lin et al. 2016; Marmanis et al. 2016; Audebert, Le Saux, and Lefèvre 2016; Audebert, Le Saux, and Lefèvre 2017; Wang et al. 2017; Kampffmeyer, Salberg, and Jenssen 2018; Liu et al. 2020), and the Agriculture-Vision benchmark dataset for automatic mapping of land pattern types (Chiu et al. 2020b; Liu et al. 2020b; Chiu et al. 2020a). In general, these architectures differ from each other in how they capture rich and global contextual information at multiple scales. For instance, the stacked UNet architecture is proposed by Ghosh et al. (2018) for land cover segmentation in remote sensing imagery, which merges high-resolution details and long range contextual information captured at low-resolution to generate segmentation maps. Further, Liu et al. (2020) introduced a dense dilated convolutions merging (DDCM) network that sequentially stacked the output of each layer with its input features before feeding it to the next layer to capture global and multi-scale contextual features.

Despite the aforementioned impressive progress on unimodal deep learning, deep learning has also been exploited for multi-modal data processing to obtain finer representations of different modalities. From the perspective of multi-modal fusion in re-

remote sensing, a multi-modal deep learning model normally involves concatenation of extracted features from unimodal networks (e.g., a backbone network) and then learning a joint representation for classification or segmentation. A representative work proposed by Audebert, Le Saux, and Lefèvre (2018) investigated two fusion strategies, namely early and late fusion methods based on the FuseNet framework, using SegNet or ResNet to classify multi-modal remote sensing data (such as LiDAR and multispectral images). Specifically, one CNN-based encoder (e.g, VGG or ResNet) is used to extract the features from RGB or IRRG images while another encoder is exploited to extract the features from LiDAR data and other bands (e.g NDVI). Note that the LiDAR data has been rasterized in the image domain as a digital surface model (DSM) with normalization (nDSM). Early fusion concatenates the features after each convolutional block from both encoders, while later fusion merges the last feature maps from the two deep networks. The results show that late fusion improves the overall accuracy at the cost of less balanced predictions, while early fusion achieves better performance for all classes but inducing higher sensitivity to missing or noisy data. Indeed, such fusion techniques do require all modalities to be available to the classification during both training and testing. Kampffmeyer, Salberg, and Jenssen (2018) therefore presented a novel CNN architecture based on so-called hallucination networks for urban land cover classification that can replace missing data modalities in the test phase. This enables fusion capabilities even when data modalities are missing in testing. Lately, Feng et al. (2019) presented an adaptive approach to fuse HSI and LiDAR data, in which a two-stream CNN is used to extract LiDAR and HSI features separately. Then an adaptive method based on squeeze-and-excitation networks (Hu, Shen, and Sun 2018) is designed to combine the features with adaptive weights instead of simply concatenation. Xu, Du, and Zhang (2018) and Xu et al. (2019) further proposed a Fusion-FCN framework for the classification of multi-source remote sensing data using fused FCNs where three different types of data (LiDAR data, hyperspectral images, and very high-resolution RGB images) are utilized in one model.

Recently, the usage of attention mechanisms in deep learning models has been increasingly explored in various visual inference tasks and has shown very promising performance gain (Fu et al. 2019; Mou and Zhu 2019; Mohla et al. 2020). Generally, the attention modules highlight the prominent features while suppressing the irrelevant features through a self-attention learning method (Vaswani et al. 2017). Recent work by Liu et al. (2020b) proposed a multi-view graph-based attention paradigm (MSCG) that demonstrated significant performance gain in contrast to a single-view attention module (SCG) (Liu et al. 2020a) for land cover mapping of multi-spectral aerial images. However, in most of these works, the attention modules are carried out only on single-level features with coarse resolution from a single modality to alleviate the computational cost. This brings challenges when attempting to accurately classify relatively small objects in very high-resolution remote sensing data. To alleviate these problems, our focus in this paper is mainly on land cover mapping (pixel-wise classification) tasks of multi-modal remote sensing images, facilitated through our proposed multi-scale and cross-view attention fusing mechanism.

3. Method

The proposed multi-modality network (MultiModNet) consists of four key modules: a backbone encoder (ENC), a pyramid attention fusion (PAF) module, a gated fusion unit (GFU), and a decoder (DEC) that produces the final output. Given a primary

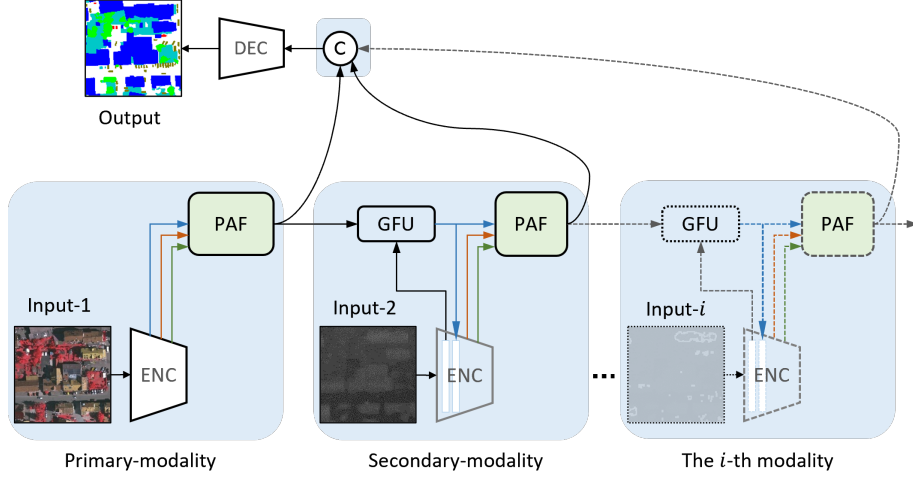


Figure 2. General concept structure of our multi-modality network (MultiModNet) based on proposed pyramid attention and gated fusion methods. Here ENC denotes the feature encoder, GFU accounts for a gated fusion unit, PAF is our proposed pyramid attention fusion module, © denotes concatenation, Input-1, Input-2 and Input- i are the primary, the secondary and the i -th modalities respectively, and, DEC is the decoder layer to output the final prediction. Note that our PAF module normally takes three different scale (i.e. 3-level) features of each modality as the input shown with blue, orange and green line.

and a secondary modality¹ Input-1 and Input-2, respectively, where Input-1, e.g. IRRG or RGB images, contains more valuable information than Input-2, e.g. DSM or NIR images, off-the-shelf encoders (ENC), such as multi-layer CNN based backbones (e.g. ResNet), are used to extract multi-level feature maps for each modality. Then we utilize PAF modules (Section 3.1) to generate fine-grained cross-level features and GFUs (Section 3.2) to merge complementary features from the primary modality into the secondary modality. Finally, we concatenate all PAF generated features from each modality and feed them into a simple decoder (DEC) module, which in this work is composed of only a single convolution layer and a bi-linear interpolation function, to output the pixel-wise classification maps. As shown in Fig. 2, our MultiModNet framework has a scalable structure that allows it to easily extend to more than two modalities. The parts that follow will go through our PAF and GFU modules in detail.

3.1. Pyramid Attention Fusion

We develop the lightweight PAF module with a built-in cross-hierarchical-scale and cross-view attention fusion mechanism that can obtain rich and robust representations. The features produced from the PAF module at each previous modality will be integrated into the encoder layer of its successor modality through a GFU module. The proposed PAF module thus plays a vital role in fusing a range of modalities in a compact yet effective manner, while it can still be used as a stand-alone decoding layer for unimodal models to improve segmentation performance.

As illustrated in Fig. 3, our PAF module contains three key sub-blocks: the pyramid cross-view encoder, the attention construction and updating block, and the feature fusion block:

¹There will be a third or even more supplementation modalities, we thus describe them using the i -th modality as illustrated in Figure 2, and assume they are ordered depending on informational richness and significance, i.e., $\text{Input-1} \geq \text{Input-2} \geq \dots \geq \text{Input-}i$. In other words, each preceding modality can be seen as a primary modality with respect to the following (succeeding, if any) ones.

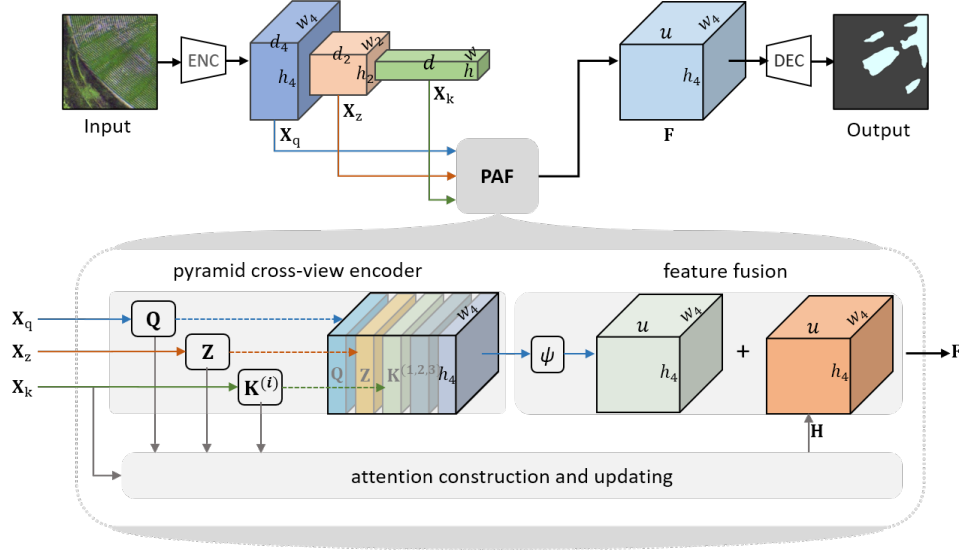


Figure 3. The illustration diagram of the pyramid attention fusion (PAF) module. Overall PAF is composed of three key blocks, i.e., the *pyramid cross-view encoder* that transforms the input pyramid features (i.e., \mathbf{X}_q , \mathbf{X}_z and \mathbf{X}_k , obtained by the ENC module) to corresponding multi-scale latent spaces (i.e., \mathbf{Q} , \mathbf{Z} and $\mathbf{K}^{(i)}$), the *attention construction and updating* block that constructs the cross-view attention matrix and then transforms the high-level features onto high-resolution 2D attention features (\mathbf{H}) by a message-passing function (see Eq. 3), and the *feature fusion* unit, which combines the latent multi-scale features with a CNN network (ψ) and sums the learned attention features (\mathbf{H}) to eventually generate the fused feature map (\mathbf{F}), which can then be fed into the DEC module to produce the final output.

- The *pyramid cross-view encoder* transforms the selected three-different-size feature maps (e.g., \mathbf{X}_q , \mathbf{X}_z , \mathbf{X}_k) to corresponding cross-level and cross-view latent representations (i.e., \mathbf{Q} , \mathbf{Z} and $\mathbf{K}^{(i)}$), in order to decrease computational burden while extracting salient latent features for late cross-view attention map generation.
- The *attention construction and updating* block constructs the cross-view and cross-level attention matrix (see Eq. 2) and then transforms the high-level features onto high-resolution 2D attention representations \mathbf{H} by a message-passing function (see Eq. 3), in order to obtain robust non-local and high-resolution contextual features.
- The *feature fusion* module combines the latent cross-level and cross-view features with a CNN network (denoted by ψ) and sums the learned high-resolution attention representation \mathbf{H} , in order to eventually produce the fine-grained contextual features \mathbf{F} , which can then be fed into the DEC module to produce the final output.

We describe each component of the framework in detail as follows.

3.1.1. Pyramid cross-view encoder

To reduce computational cost while obtaining robust latent feature representations for late constructing attention maps, we utilize a multi-view augmenting method (Liu et al. 2020b) in the pyramid cross-view encoder to explicitly exploit the rotation invariance in the deep features. We first define a view generation function $\mathbf{X}_k^{(i)} = \tau(\mathbf{X}_k, i)$, and a view reversion function $\mathbf{X}_k = \tau^{-1}(\mathbf{X}_k^{(i)}, i)$ for three different views ($i \in \{1, 2, 3\}$).

We let $\mathbf{X}_k^{(1)} = \mathbf{X}_k$, and generate $\mathbf{X}_k^{(2)}$ and $\mathbf{X}_k^{(3)}$ by transposing and vertically flipping, respectively. Then the module learns pyramid-level and cross-view latent representations, i.e., a low-level feature matrix $\mathbf{Q} \in \mathbb{R}^{h_4 \times w_4 \times c}$, a middle-level latent matrix $\mathbf{Z} \in \mathbb{R}^{h_2 \times w_2 \times c}$ and the high-level 3-view matrix $\mathbf{K}^{(i)} \in \mathbb{R}^{h \times w \times c}$ from the multi-scale features $\mathbf{X}_q \in \mathbb{R}^{h_4 \times w_4 \times d_4}$, $\mathbf{X}_z \in \mathbb{R}^{h_2 \times w_2 \times d_2}$, and $\mathbf{X}_k \in \mathbb{R}^{h \times w \times d}$, respectively, using CNNs, i.e.,

$$\mathbf{Q} = \varphi(\mathbf{X}_q; \boldsymbol{\theta}_q), \quad \mathbf{Z} = \varphi(\mathbf{X}_z; \boldsymbol{\theta}_z), \quad \text{and} \quad \mathbf{K}^{(i)} = \tau^{-1} \left(\varphi(\mathbf{X}_k^{(i)}; \boldsymbol{\theta}_k), i \right), \quad (1)$$

where φ denotes the convolution layers with parameter kernels of $\boldsymbol{\theta}_q \in \mathbb{R}^{d_4 \times 3 \times 3 \times c}$, $\boldsymbol{\theta}_z \in \mathbb{R}^{d_2 \times 3 \times 3 \times c}$, and $\boldsymbol{\theta}_k \in \mathbb{R}^{d \times 3 \times 3 \times c}$ respectively. Note that d_4 , d_2 , and d represent the input feature dimensions of \mathbf{X}_q , \mathbf{X}_z and \mathbf{X}_k respectively, c is the output feature dimension, and typically $c < d_4 < d_2 < d$. Here, $h_4 \times w_4$, $h_2 \times w_2$ and $h \times w$ denote the spatial sizes of both the input and the output feature maps, and commonly $h_4 = 2h_2 = 4h$, $w_4 = 2w_2 = 4w$. We also use zero-padding methods in CNN layers of the module to keep the output spatial resolution the same as the input.

3.1.2. Attention construction and updating

To obtain a robust non-local and high-resolution contextual feature space based on these learned three-level and three-view latent representations (i.e., \mathbf{Q} , \mathbf{Z} , $\mathbf{K}^{(i)} : i = 1, 2, 3$), we propose a novel attention construction and updating module that can efficiently model long-range and cross-level pixel-wise dependencies and effectively produce rich non-local and high-resolution contextual representations via an upsampling-based attention-passing mechanism. This module is formed of two key components: attention construction and attention-passing. They are described in detail as follows.

Attention construction. Inspired by the success of self-attention (Vaswani et al. 2017) to encode the structural information of a sequence of data, we present a long-range cross-level attention method that uses latent feature similarity to model the interactions between every pair of pixels in cross-level feature maps. Furthermore, we introduce a multi-view fusion strategy in the attention module, which allows us to encode cross-level as well as cross-view pixel-wise dependencies to improve its robustness. Specifically, we first reshape the low-level high-resolution latent matrix \mathbf{Q} to $\hat{\mathbf{Q}} \in \mathbb{R}^{(h_4 w_4) \times c}$, the middle-level latent matrix \mathbf{Z} to $\hat{\mathbf{Z}} \in \mathbb{R}^{(h_2 w_2) \times c}$ and the high-level view matrices $\mathbf{K}^{(i)}$ to $\hat{\mathbf{K}}^{(i)} \in \mathbb{R}^{(hw) \times c}$. Then our cross-view and cross-level attention construction function is defined as

$$\mathbf{A} = \text{norm} \left(\overbrace{\sum_{i=1}^3 w_i \text{ReLU} \left(\hat{\mathbf{Q}} \left(\underbrace{\tanh(\hat{\mathbf{Z}}^\top \hat{\mathbf{Z}}) + \mathbf{I}_\alpha}_{\text{channel-wise attention}} \right) \hat{\mathbf{K}}^{T(i)} \right)}^{\text{cross-view fusion}} \right) \in \mathbb{R}^{(h_4 w_4) \times (hw)} \quad (2)$$

where w_i is a learnable parameter initialized as 1 for our attention construction function, $\tanh(\cdot)$ and $\text{ReLU}(\cdot)$ denote the tanh and ReLU non-linear functions respectively, and $\mathbf{I}_\alpha \in \mathbb{R}^{c \times c}$ is a learnable bias kernel initialized as \mathbf{I} . Note that the attention matrix \mathbf{A} is constructed from features from different scales, resulting in long-range cross-level attention. The matrix is therefore a tall matrix, i.e. it has more rows (e.g., $16hw$) than

columns (e.g., hw), and it is further normalized, i.e. $\text{norm}(\cdot)$, along rows by dividing by the sum of each row, so that the elements of each row vector in the matrix add up to 1. Figure 4 illustrates the attention matrix constructing process.

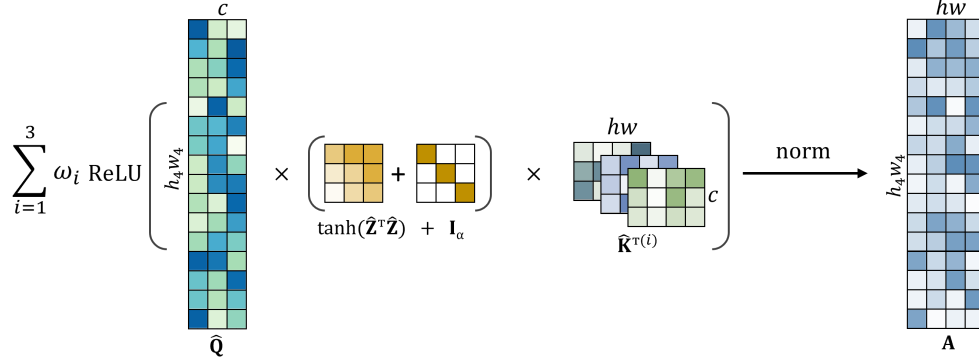


Figure 4. The illustration of attention construction

Note that our attention construction process differs from the self-attention scheme in three major ways, i.e.,

- *Cross-level attention:* Our cross-level attention scheme utilizes three distinct level feature maps as the sources of multi-scale latent representations to efficiently generate a tall non-local interaction matrix instead of a square self-attention matrix. This allows our attention module to learn high-resolution features from low-resolution but high-abstract feature space. Based on our observations, using our cross-level attention to capture contextual information leads to faster training and better performance on remote sensing data than using self-attention methods based on one-scale low-resolution features or image patches (Dosovitskiy et al. 2021).
- *Channel-wise attention:* We also integrate a channel-wise attention method, i.e., $\tanh(\hat{\mathbf{Z}}^T \hat{\mathbf{Z}}) + \mathbf{I}_\alpha$, into our long-range cross-level attention scheme (see Eq. 2) to improve feature discriminability by blending channel-wise weights learned from the middle-level feature (\mathbf{Z}) space. We observe that this results in better training stability and less sensitivity to latent feature dimensionalities (i.e., c) when compared to not using the channel-wise attention mechanism. We think that the channel-wise attention, like the dual attention network (Fu et al. 2019), could enhance our long-range attention mechanism by merging both channel and spatial attention attributes to capture robust cross-level information.
- *Cross-view fusion:* Furthermore, we introduce a cross-view fusion strategy into our attention module, inspired by our previous work (Liu et al. 2020b), to explicitly encode the rotation invariance in the high-abstract and deep-level latent features (i.e., \mathbf{K}). We fuse (add up) three-view long-range attention maps using learnable weights (i.e., w_i in Eq. 2) to further improve the model’s robustness. Base on our experiments, using cross-view attentions can further speed up the model’s learning process and result in better performance than using single-view attention maps.

Attention-passing. To produce a non-local but high-resolution feature representation (i.e., \mathbf{H} : typically 4 times the size of \mathbf{X}_k) from the high-level but low-resolution features \mathbf{X}_k , we develop an upsampling-based attention-passing function $f(\cdot)$ (Eq. 3). It

is parameterized by the normalized attention matrix \mathbf{A} and \mathbf{X}_k with trainable parameters $\mathbf{W} \in \mathbb{R}^{d \times u}$ where u denotes the output feature dimension. Our attention-passing mechanism, i.e., $\mathbf{A}\hat{\mathbf{X}}_k\mathbf{W}$, is similar to the one-hop neighborhood message-passing function of graph convolutional networks (Kipf and Welling 2016) when viewing our learned tall attention matrix as a special type of adjacency matrix. Note that $\hat{\mathbf{X}}_k \in \mathbb{R}^{(hw) \times d}$ is obtained by reshaping of \mathbf{X}_k .

$$\mathbf{H} = f\left(\mathbf{X}_k \in \mathbb{R}^{h \times w \times d}; \mathbf{A}, \mathbf{W}\right) = \delta\left(\mathbf{A}\hat{\mathbf{X}}_k\mathbf{W}\right) \in \mathbb{R}^{h_4 \times w_4 \times u}. \quad (3)$$

With a combination operator, denoted by $\delta(\cdot)$ in Eq. 3, of non-linear activation function (e.g. ReLU) with bath normalization and reshaping, we eventually obtain a high-resolution attention representation $\mathbf{H} \in \mathbb{R}^{h_4 \times w_4 \times u}$ as illustrated in Figure 5.

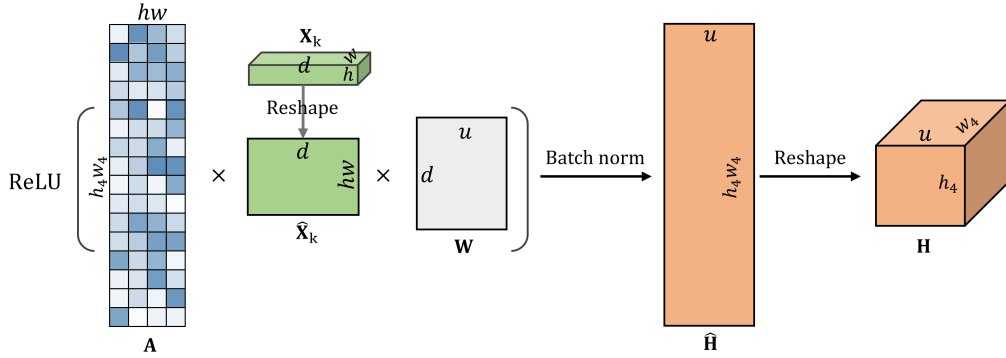


Figure 5. The illustration of attention-passing pipeline.

3.1.3. Feature fusion

Finally, we fuse the high-resolution attention features with cross-level and cross-view latent features in order to produce fine-grained high-resolution representations with robust non-local contextual and spatial information as the output using

$$\mathbf{F} = \psi\left(\mathbf{Q} \parallel \tilde{\mathbf{Z}} \parallel \tilde{\mathbf{K}}^{(1)} \parallel \tilde{\mathbf{K}}^{(2)} \parallel \tilde{\mathbf{K}}^{(3)}; \boldsymbol{\theta}_\psi\right) + \mathbf{H}, \quad (4)$$

where ψ denotes the convolution layer with parameter kernels of $\boldsymbol{\theta}_\psi \in \mathbb{R}^{5c \times 3 \times 3 \times u}$, batch normalization and non-linearity, and \parallel denotes concatenation. Please note that middle-level latent and high-level view feature matrices (\mathbf{Z} and $\mathbf{K}^{(i)}$) are up-sampled using bi-linear interpolation to $\tilde{\mathbf{Z}}$ and $\tilde{\mathbf{K}}^{(i)}$ in order to match the dimension of the high-resolution (i.e. $h_4 \times w_4$) feature matrix \mathbf{Q} for concatenating. This is similar to the multi-level feature fusion method of pyramid feature networks (FPNs) (Lin et al. 2017), which fuse multi-level features from the top-down path by upsampling and summing, but instead of summation, we use concatenation and convolution operations to merge multi-level feature maps for remote sensing data.

3.2. Gated Fusion Unit

The GFU module is designed to serve as a fusion gateway between the main and secondary modalities. It utilizes a novel gating mechanism to allow the primary modality to aid its secondary modality in extracting the supplementary information via a gating network, thereby minimizing the influence of hidden noise and redundancies. Specifically, the GFU module is composed of two CNN layers with two gating operations (element-wise multiplications) as shown in Fig. 6. The first gate operation helps to weaken redundancies and capture salient useful features from the secondary modality, while the second gate operation aims to obtain complementary features from the primary modality and merge them into the secondary modality. The operation of the

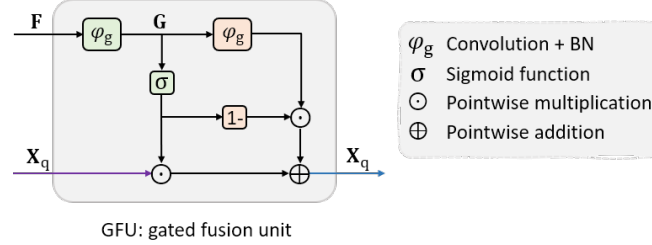


Figure 6. The gated fusion unit (GFU) consists of 2 CNN layers (φ_g) with batch normalization, and an activation function (σ , i.e., Sigmoid), where '1-' denotes one minus the input activation maps.

GFU module can be summarized by the following mathematical equations:

$$\mathbf{G} = \varphi_g(\mathbf{F}; \boldsymbol{\theta}_s), \quad \mathbf{X}_q = \sigma(\mathbf{G}) \odot \mathbf{X}_q + (1 - \sigma(\mathbf{G})) \odot \varphi_g(\mathbf{G}; \boldsymbol{\theta}_r), \quad (5)$$

where \mathbf{F} represents the fused representations by the PAF module of the primary modality and \mathbf{X}_q denotes the low-level features extracted by the encoder of the secondary modality. Here φ_g represents the convolution layers with 1×1 filters $\boldsymbol{\theta}_s$ and $\boldsymbol{\theta}_r$ respectively, and combine a batch normalization operator. σ is a sigmoid activation function. Note that the updated \mathbf{X}_q (the output of GFU) will feed the remaining layers of the encoder and also serve as one of the three input feature maps to the PAF module.

4. Data, experiments and results

4.1. Benchmark datasets

In this paper, we focus on two different representative databases, namely the ISPRS Vaihingen 2D dataset (Rottensteiner et al. 2012) and the Agriculture-Vision² challenge dataset (Chiu et al. 2020b). The ISPRS Vaihingen 2D dataset³ is comprised of aerial remote sensing images over the city Vaihingen in Germany. The Agriculture-Vision dataset consists of large-scale high-quality aerial images from 3,432 farmlands across the US and has been annotated with nine types of field anomaly patterns that are most important to farmers. Each dataset provides online leaderboards and reports test metrics measured on hold-out test images.

²<https://www.agriculture-vision.com/agriculture-vision-2021/dataset-2021>

³<http://www2.isprs.org/commissions/comm3/wg4/2d-sem-label-vaihingen.html>

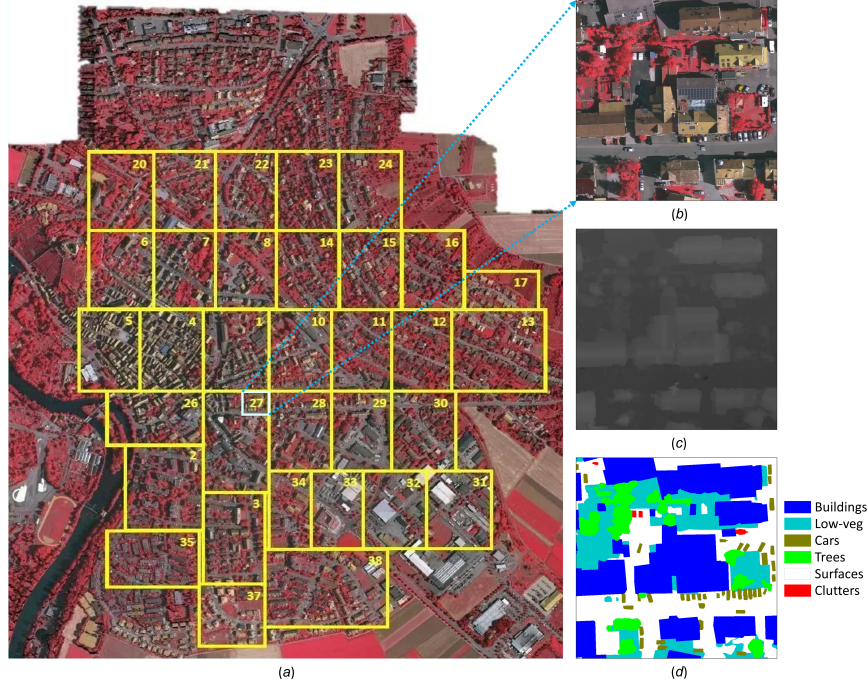


Figure 7. Overview of the ISPRS Vaihingen 2D semantic labeling benchmark dataset that contains 33 tiles: (a) overview of the entire dataset (the ID number labeled in the upper right corner of each area), (b) the IRRG image patch, (c) the DSM, (d) the ground truth.

4.1.1. Vaihingen dataset

The Vaihingen dataset is composed of 33 orthorectified image tiles acquired by a near-infrared (NIR) - red (R) - green (G) aerial camera and has been labeled with six common land cover categories: impervious surfaces (i.e., roads and concrete surfaces), buildings, low vegetation, trees, cars and clutter (representing uncategorizable land covers). 16 out of the 33 tiles are fully annotated at pixel level as the training set, and 17 tiles (i.e., areas: 2, 4, 6, 8, 10, 12, 14, 16, 20, 22, 24, 27, 29, 31, 33, 35 and 38) are used as hold-out test images as shown in Fig. 7. The average size of the tiles is approximately 2500×2000 pixels with a ground resolution of 9cm.

Images are accompanied by a digital surface model (DSM) that is derived from dense image matching techniques and represents the absolute height of pixels. Normalized DSM (nDSM) data are also included, which represent the pixels heights relative to the elevation of the nearest ground surface. We use both IRRG and nDSM data for training and test. Fig. 7 shows some examples of the dataset.

4.1.2. Agriculture-Vision dataset

The Agriculture-Vision dataset consists of 94,986 aerial farmland images, of which 19,708 images are used as the hold out test set, and 18,334 are used as the local validation set. Each image consists of 512×512 RGB and NIR channels with resolution as high as 10 cm per pixel. Nine types of the most important field patterns are annotated: double plant, drydown, endrow, nutrient deficiency, planter skip, storm damage, water, waterway, and weed cluster. In addition, each image has a boundary map that indicates the region of the farmland, and a mask that indicates valid pixels in the image. Fig. 8 shows some examples of the dataset (note that the black regions

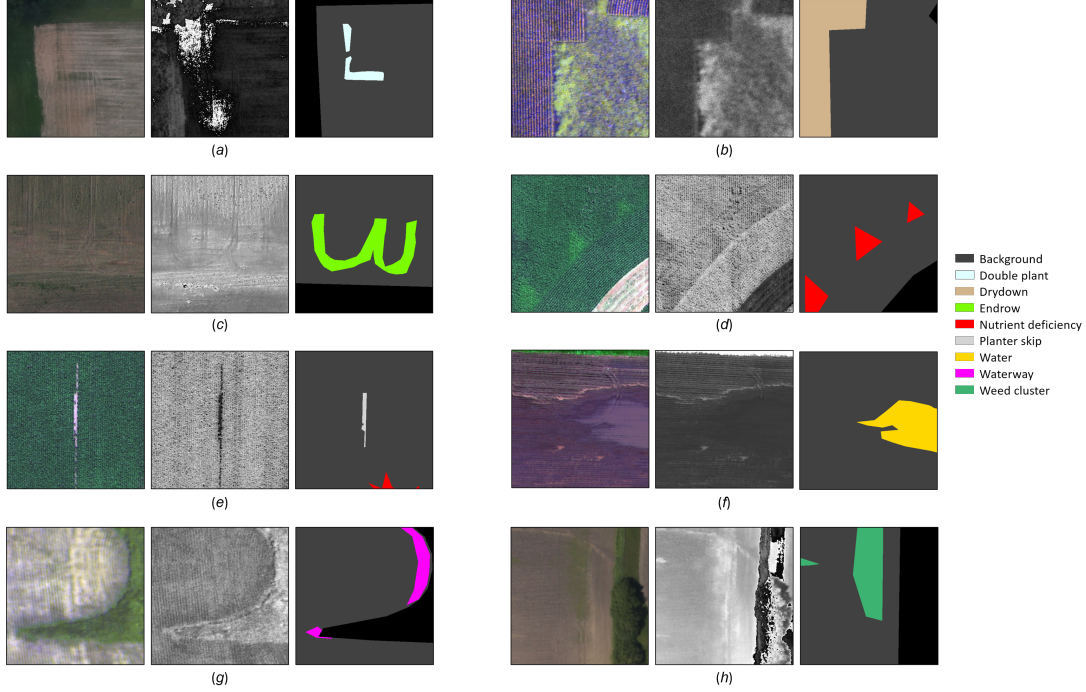


Figure 8. Some image examples of the agriculture-vision dataset: (a) the double plant patches (left: RGB image, middle: NIR image, right: the ground truth), (b) the drydown patches, (c) the endrow patches, (d) the nutrient deficiency patches, (e) the planter skip patches, (f) the water patches, (g) the waterway patches, (h) the weed cluster patches.

in the ground truth denote invalid areas).

Due to the fact that some annotations may overlap in the dataset, for pixels with multiple labels, a prediction of either label will be counted as a correct pixel classification for that label. Therefore, the conventional mean Intersection-over-Union (mIoU) metric is modified accordingly by categorizing predictions of any label in a pixel as a correct prediction. This customized mIoU is used as the main quantitative evaluation metric of the contest dataset (Chiu et al. 2020a).

4.2. Variants of MultiModNet

Built upon PAF, GFU, and the incorporation of different backbone encoders, we develop various MultiModNet models for land cover mapping tasks on different remote sensing data as shown in Table 1. Specifically, we use different backbone encoders

Table 1. Detailed configurations of variants of MultiModNet with quantitative comparison of parameters size, FLOPs (measured on input image size of $4 \times 512 \times 512$), Inference time on CPU and GPU separately.

Models	Inputs	ENC-1	ENC-2	PAF-1	PAF-2	GFU	Parameters (Million)	FLOPs (Giga)	Inference time (ms - CPU/GPU)
PAFNet ^a	DSM-IRRG (unimodal 4-band)	Se_ResNext50 (output: 256/512/1024)	\times	latent:6 output:24	\times	\times	9.52	18.12	513 / 24
PAGNet ^a	IRRG, DSM (Two-modal)	Se_ResNext50 (output: 256/512/1024)	MobileNetV3 (output: 40/112/960)	latent:6 output:24	latent:6 output:24	output:40	12.62	21.34	564 / 36
PAFNet ^b	NIR-RGB (unimodal 4-band)	MobileNetV3 (output: 40/112/960)	\times	latent:8 output:32	\times	\times	4.86	5.23	68 / 6
PAGNet ^b	RGB, NIR (Two-modal)	MobileNetV3 (output: 40/112/960)	MobileNetV3 (output: 40/112/960)	latent:8 output:32	latent:8 output:32	output:40	6.14	7.86	127 / 11

(all are pretrained on ImageNet in this work) for Vaihingen and Agriculture-vision datasets. Our models, i.e., PAFNet^a and multi-modal PAGNet^a for the Vaihingen dataset, use the Se_ResNext50 (Hu, Shen, and Sun 2018) as the ENC-1 for IRRG images and the MobileNetV3 (Howard et al. 2019) as ENC-2 for DSM data respectively, while for the Agriculture-Vision dataset, the models i.e. PAFNet^b and PAGNet^b, we use two identical MobileNetV3 models as the encoders for both RGB and NIR data. We were not able to use Se_ResNext50 for the Agriculture-Vision dataset due to the memory limitation (11Gb) of our GPU, since Se_ResNext50 requires much more memory compared to MobileNetV3 when taking larger input size and batch size required for training models on the Agriculture-vision dataset.

4.3. Training details

According to best practices, we train all our models using Adam (Kingma and Ba 2014) as the optimizer for the first 10k iterations and then change the optimizer to SGD in the remaining iterations with weight decay 2×10^{-5} applied to all learnable parameters except biases and batch-norm parameters. We use a polynomial learning rate (lr) decay $(1 - \frac{cur_iter}{max_iter})^{0.9}$ with the maximum iterations set to 10^8 . We also set $2 \times lr$ to all bias parameters in contrast to weights parameters. Based on our training observations to achieve fast and stable convergence, we apply the adaptive multi-class weighting loss (\mathcal{L}_{acw}) function (Liu et al. 2020b) for all our experiments.

Guided by our empirical results and our previous work (Liu et al. 2020; Liu et al. 2020b), we train and validate the networks for the Vaihingen dataset with 5000 randomly sampled patches of size 448×448 as input and a batch size of five. For the experiments on the Agriculture-Vision dataset, we randomly sample images of size 512×512 as input and train it using mini-batches of size 12. We conduct all experiments using PyTorch on a computer with a single GeForce GTX 2080Ti. For the Vaihingen dataset, we set the initial learning rate to 1.8×10^{-4} and utilized a step-wise learning-rate schedule method that reduces the learning rate by a factor of 0.75 every 5 epochs based on our training observations and empirical evaluation, while for Agriculture-vision models, we use initial learning rates of 2.8×10^{-4} and apply a cosine annealing scheduler that reduces the learning rates over epochs (for a maximum epoch of 40).

4.4. Augmentation and evaluation methods

During training, all data is sampled uniformly and augmented with random flip (horizontal and vertical), rotation (90 degree), Gaussian noise, and brightness contrast (all probabilities are 0.5) for each epoch. The albumentations library (Buslaev et al. 2020) for data augmentation is utilized in this work. Please note that all training images are normalized to $[0.0, 1.0]$ after data augmentation.

During test and evaluation, we apply test time augmentation (TTA) in terms of flipping and mirroring. For Vaihingen data, we use sliding windows (with 448×448 size at a 100-pixel stride) on a test image and stitch the results together by averaging the predictions of the over-lapping TTA regions to form the output. For the agriculture-vision data, we first apply TTA on the full size test image (512×512) and average the predictions to get the final output. The performance is measured by the F1-score for Vaihingen dataset, and the modified Intersection over Union (IoU) (Chiu et al. 2020a) for the agriculture-vision dataset. Please note that the mIoU metric was computed by

averaging over the nine classes (including the 'Background' class) in the Agriculture-Vision benchmark dataset.

4.5. Test results

We tested our trained models on the hold out test sets of the Vaihingen and Agriculture-Vision datasets. The test results are shown in Table 2 and Table 3, respectively. It is clearly visible for all the cases that our method outperforms all the state-of-the-art methods with a significant margin. For the Vaihingen dataset, it can be seen that the accuracy for the 'Car' class (90.8% F1-score) is notably improved (+2.5%) using our method in comparison to other methods. In case of the Agriculture-Vision dataset, many difficult classes also show significant increases in terms of IoU accuracies, e.g., double plant (+9.4%), drydown (+5.8%), endrow (+8.2%), and planter skip (+5.3%), etc.

A qualitative comparison of the segmentation results from our trained models and the ground truths on the validation data are shown in Fig. 9 and Fig. 10. It can be visually verified that the classification maps obtained from our PAG-Net models tend to be less noisy and have smooth and fine-gained boundary recovery without any post-processing. In addition, our multi-modal PAGNet^b model obtained the best performance on the Agriculture-Vision dataset with 48.2% mIoU (+4.2%) with fewer training parameters (6.14M) and 2× faster training and inference speed on both CPU (127ms) and GPU (11ms) in comparison to MSCG-Net50 as shown in Table 1. It is worth noting that our two PAF-base unimodal models (PAFNet^a and PAFNet^b) also obtain the best performance compared to other unimodal methods on both the Vaihingen and Agriculture-Vision datasets.

Table 2. Comparisons between our method with other published methods on the hold-out test images of Vaihingen Dataset.

Models	OA	Surface	Building	Low-veg	Tree	Car	mF1
UOA (Lin et al. 2016)	0.876	0.898	0.921	0.804	0.882	0.820	0.865
DNN.HCRF (Liu et al. 2019)	0.878	0.901	0.932	0.814	0.872	0.720	0.848
ADL3 (Paisitkriangkrai et al. 2015)	0.880	0.895	0.932	0.823	0.882	0.633	0.833
DST_2 (Sherrah 2016)	0.891	0.905	0.937	0.834	0.892	0.726	0.859
ONE_7 (Audebert, Le Saux, and Lefèvre 2016)	0.898	0.910	0.945	0.844	0.899	0.778	0.875
DLR_9 (Marmanis et al. 2016)	0.903	0.924	0.952	0.839	0.899	0.812	0.885
GSN (Wang et al. 2017)	0.903	0.922	0.951	0.837	0.899	0.824	0.887
RWSNet (Jiang et al. 2020)	0.899	0.916	0.947	0.840	0.893	0.860	0.891
DDCM-R50 (Liu et al. 2020)	0.904	0.927	0.953	0.833	0.894	0.883	0.898
SCG-GCN (Liu et al. 2020b)	0.904	0.924	0.948	0.839	0.897	0.880	0.898
FuseNet (IRRG+DSM/NDVI)	0.908	0.913	0.943	0.848	0.899	0.859	0.901
PAFNet ^a (DSM-IRRG)	0.906	0.929	0.949	0.826	0.894	0.905	0.900
PAGNet ^a (IRRG+DSM)	0.913	0.930	0.952	0.843	0.900	0.908	0.907

Table 3. Comparisons between our method with other published methods in terms of mIoUs and class IoUs on the hold-out Agriculture-Vision test set.

Models	mIoU	Background	Double plant	Drydown	Endrow	Nutrient deficiency	Planter skip	Water	Waterway	Weed cluster
DeepLabv3(os=8)	0.322	0.704	0.215	0.510	0.126	0.394	0.204	0.157	0.337	0.250
DeepLabv3+(os=8)	0.391	0.710	0.197	0.509	0.195	0.413	0.244	0.623	0.341	0.280
DeepLabv3+(os=16)	0.422	0.727	0.252	0.536	0.210	0.440	0.246	0.704	0.386	0.299
DeepLabv3+(os=16)	0.424	0.725	0.260	0.536	0.241	0.442	0.244	0.703	0.379	0.288
FPN-ResNet (Chiu et al. 2020b)	0.437	0.726	0.279	0.523	0.243	0.438	0.310	0.713	0.388	0.309
MSCG-Net50 (Liu et al. 2020b)	0.441	0.716	0.289	0.513	0.270	0.442	0.331	0.692	0.366	0.349
PAFNet ^a (IR-RGB)	0.442	0.687	0.343	0.562	0.281	0.420	0.305	0.680	0.378	0.324
PAGNet ^b (RGB+IR)	0.482	0.740	0.383	0.581	0.352	0.460	0.384	0.686	0.373	0.379

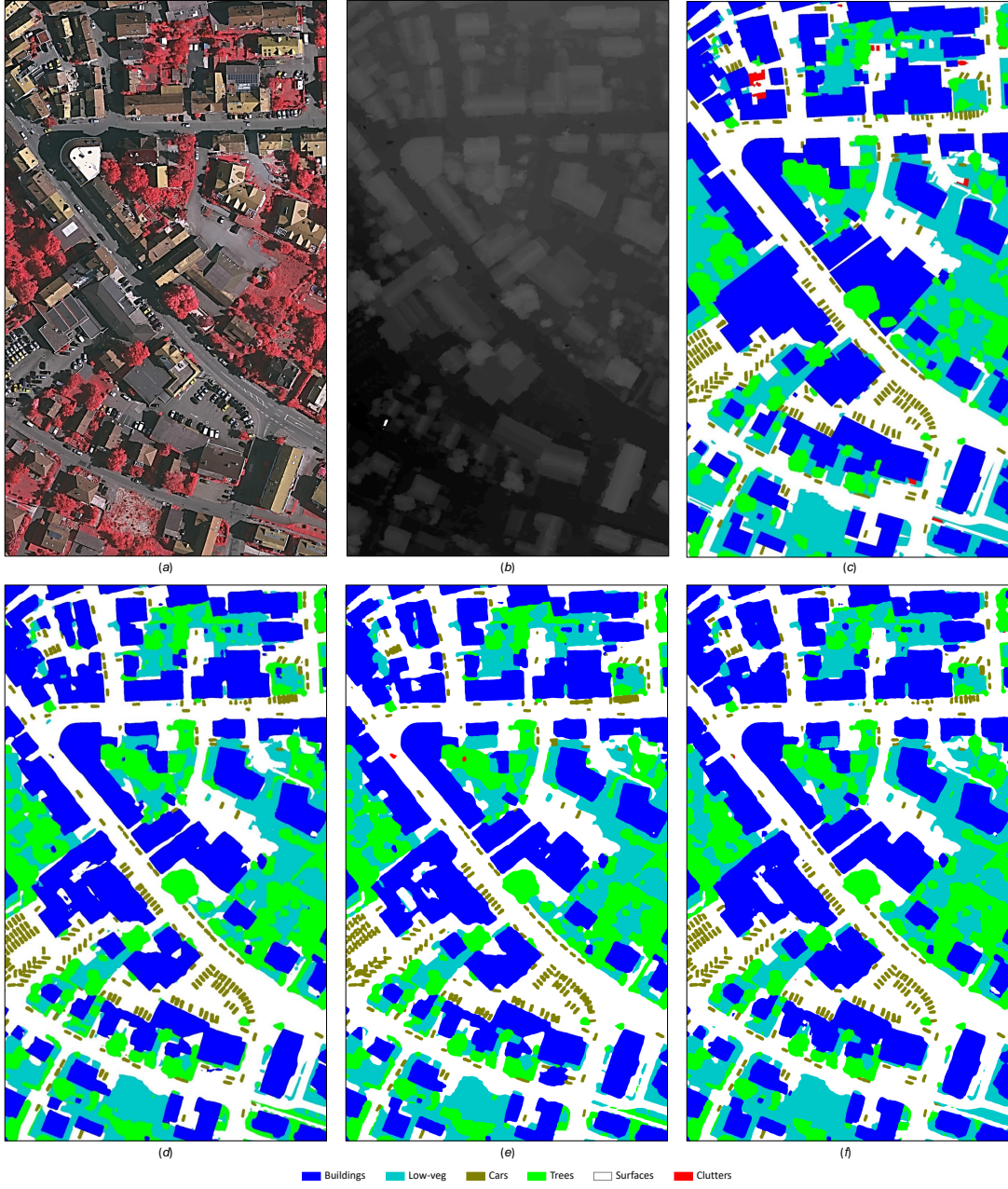


Figure 9. Segmentation results for the test image of Vaihingen tile-27: (a) the test IRRG image, (b) the DSM image, (c) the ground truth, (d) DDCM-R50, (e) SCG-GCN, (f) PAGNet^a

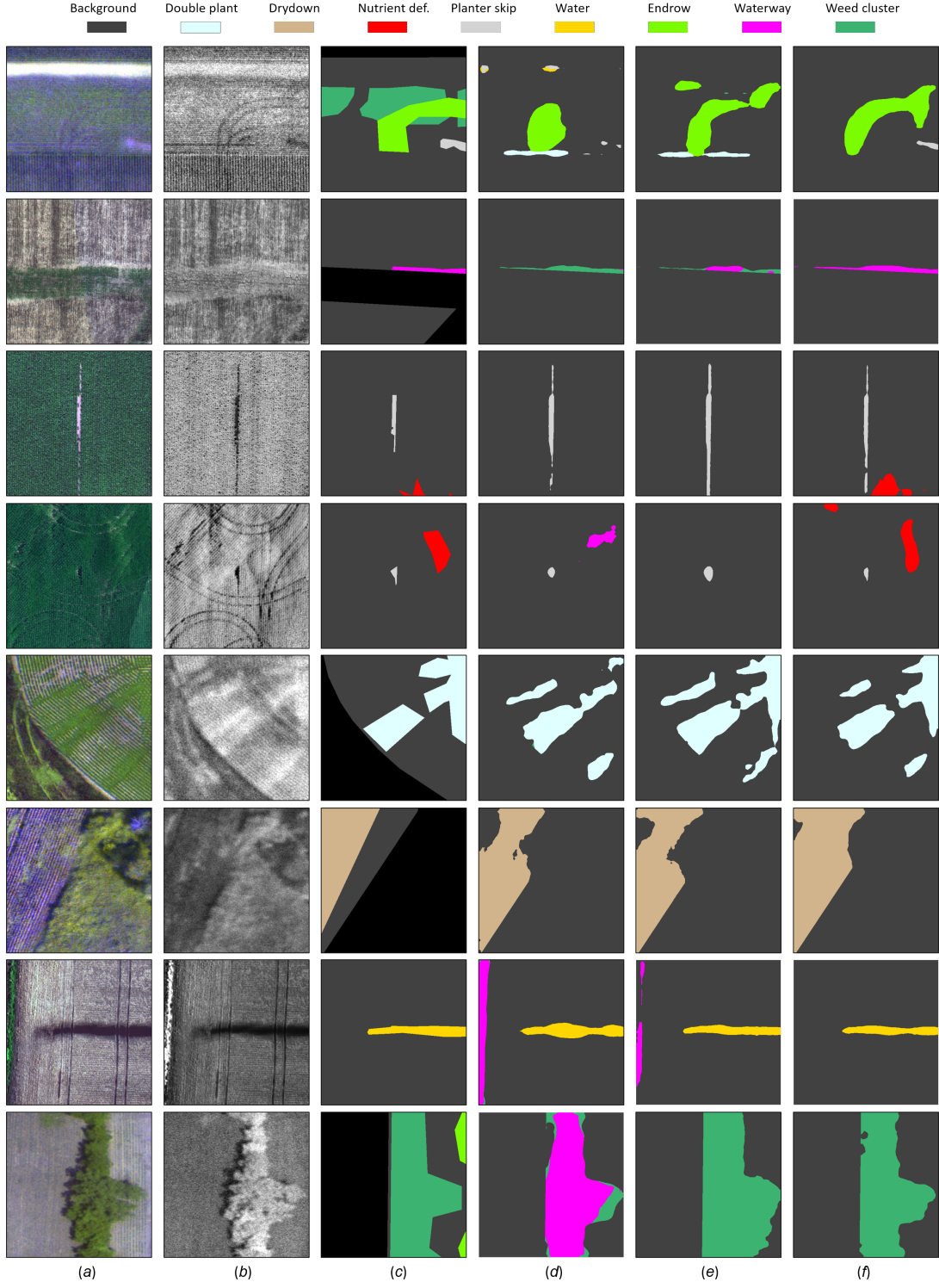


Figure 10. Segmentation results on the validation images of the agriculture-vision dataset: (a) the RGB images, (b) the NIR images, (c) the ground truth, (d) MSCG-Net50, (e) PAFNet^b, (f) PAGNet^b

5. Discussion

In our network, pyramid attention fusion (PAF) modules are employed to capture multi-level and cross-view robust representations, and gated fusion units (GFU) are designed to bridge and interact among different modalities to better combine multi-modality information. To validate the effectiveness of these modules, we perform ablation experiments on the Vaihingen dataset.

5.1. Effect of the pyramid attention fusion module

In Table 4, we evaluate our model’s performance by removing the key components of the PAF module, i.e., pyramid cross-view encoder (PCE), attention construction and updating (ACU) module as shown in Fig. 3. Since PCE and ACU are interdependent, we are not able to just use ACU without the PCE unit. We, therefore, evaluated the following two variations: 1) V-1: replacing both PCE and ACU with using multi-level concatenation fusion networks (FPN-style) with the same number of hidden features of the PAF module. 2) V-2: only removing ACU module. It is evidently shown that in absence of our pyramid attention fusion module, the V-1 model tends to underperform a lot on small objects (e.g., ‘Car’ -4.8%), while only applying our pyramid cross-view encoder block, our V-2 model improves the performance a bit overall (mF1: $+0.9\%$ in contrast to V-1 model) but still underperforms on the small class ‘Car’ (mF1: -2.4% in contrast to PAGNet).

Table 4. The effect of the two key units (PCE, ACU) of our PAF module on the hold-out test images of Vaihingen Dataset.

Model	PCE	ACU	OA	$\Delta\%$	Building	$\Delta\%$	Car	$\Delta\%$	mF1	$\Delta\%$	Steps (K)
V-1	\times	\times	0.898	-1.5	0.942	-1.0	0.860	-4.8	0.890	-1.7	31
V-2	\checkmark	\times	0.906	-0.7	0.945	-0.7	0.884	-2.4	0.899	-0.8	25
PAGNet	\checkmark	\checkmark	0.913	-	0.952	-	0.908	-	0.907	-	29

We also investigated the effect of the latent features and cross-view settings on the performance. Note that, we assume that the number of latent features (c) should be close to the number for classes (i.e., 6 for Vaihingen dataset). The latent features are thus set to be in the range of $\{4, 6, 8, 12\}$, and the number of views (v) are in the range of $\{1, 2, 3\}$. Table 5 presents the details of the evaluation results where five models are trained on various latent features and cross-view settings. Our model with latent features of 6 and view number of 3 achieves the best results. Note that the latent feature number does not show a significant impact on overall performance (mF1: $\pm 0.5\%$), while the number of views seems to be more sensitive on both overall results (mF1: $\pm 1.0\%$) and the performance on small objects (mF1: $\pm 2.9\%$).

Table 5. The effect of different the number of latent features and views of our PAF module on the hold-out Vaihingen test set.

Model	c	v	OA	$\Delta\%$	Building	$\Delta\%$	Car	$\Delta\%$	mF1	$\Delta\%$	Steps (K)
PAG-v1	4	3	0.907	-0.6	0.950	-0.2	0.904	-0.4	0.903	-0.4	35
PAG-v2	8	3	0.910	-0.3	0.957	+0.3	0.905	-0.3	0.904	-0.3	21
PAG-v3	12	3	0.908	-0.5	0.952	0	0.891	-1.7	0.902	-0.5	17
PAG-v4	6	1	0.902	-1.1	0.947	-0.5	0.879	-2.9	0.897	-1.0	19
PAG-v5	6	2	0.909	-0.4	0.949	-0.3	0.898	-1.0	0.904	-0.3	23
PAGNet	6	3	0.913	-	0.952	-	0.908	-	0.907	-	29

* c is the number of latent features and v denotes the number of views. Here Steps K=1000 denote training iterations.

5.2. Effect of the gated fusion unit

The GFU module plays a very important role for the effectiveness and efficiency of our multi-modal PAGNet. We, therefore, evaluate GFU by comparing it with the other two commonly used fusion methods (i.e., element-wise summing, and concatenation). Table 6 displays the performance of these three methods. It is clearly shown that simply concatenating or summing multi-modality features will cause a degradation in performance to unimodal models. Our GFU approach, instead, shows notable performance gains (mF1: +1.1 ~ 1.4%) in general and significantly boosts the results on small objects (mF1: +2.2 ~ 3.3%) and improves the training converges speed (+2x faster). We visualized the GFU module learned attention gate map as shown in Figure 11. It illustrates that GFU module is able to capture a significant or complementary part of the information contained in the DSM data and diminish the influence of noisy data as well.

Table 6. Test performance of different fusion settings on Vaihingen test set.

\oplus	\odot	\otimes	OA	$\Delta\%$	Building	$\Delta\%$	Car	$\Delta\%$	mF1	$\Delta\%$	Steps (K)	Δ
\checkmark			0.901	-1.2	0.950	-0.2	0.875	-3.3	0.893	-1.4	67	2.3x
	\checkmark		0.906	-0.7	0.946	-0.6	0.886	-2.2	0.896	-1.1	92	3.1x
		\checkmark	0.913	-	0.952	-	0.908	-	0.907	-	29	-

* \oplus denote point-wise summing fusion, \odot is concatenation fusion, and \otimes is our gated fusion method.

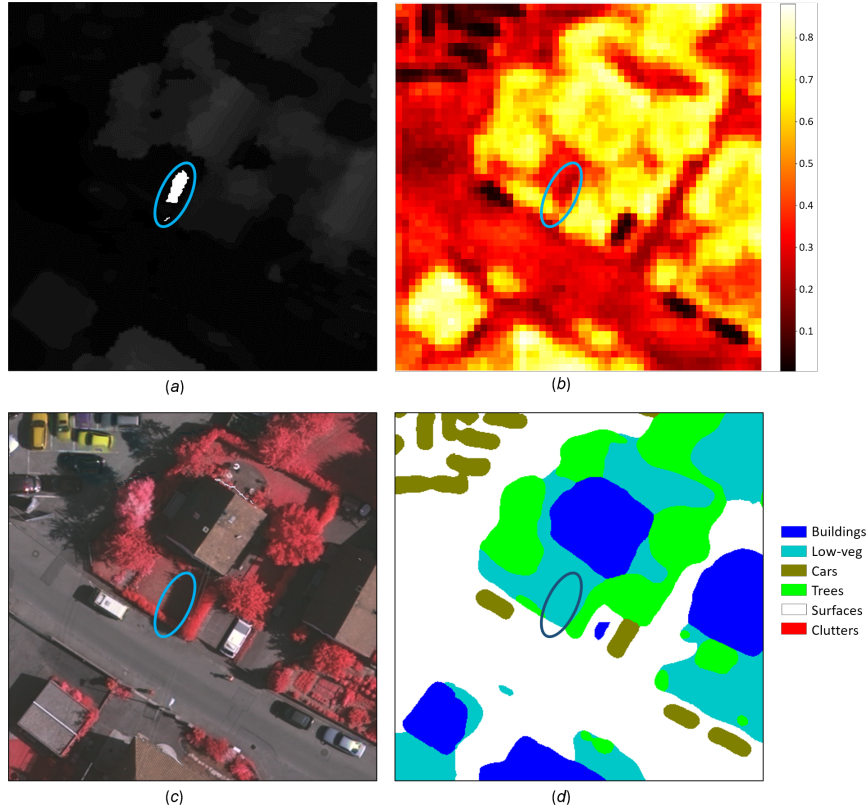


Figure 11. Heatmap of the GFU learned attention gate : (a) the DSM image (containing some noisy patch), (b) the attention gate heatmap, (c) the IRRG image, (d) the prediction.

5.3. Effect of missing and noisy data

We also evaluate the performance of our model to handle situations where DSM data are missing, noisy and completely interfered during testing. Specifically, we assume that the IRRG data modality of the Vaihingen dataset is available, while the DSM modality is missing (letting DSM data to 0), random noisy signal (using white noise data sampled from 0 to 255), or completely interfered (setting data value to 255). Table 7 illustrates the results. It clearly indicates that our model is capable of dealing with missing or noisy data. In other words, our model, which was trained with all data modalities (e.g., IRRG+DSM), generalizes well to circumstances in which extra modality data (e.g, DSM) is absent or entirely noisy during the testing phase. Our model’s weakness for missing and noisy data modalities is that it does not handle missing primary modalities adequately (e.g., IRRG or RGB). In many situations, this is not an issue because it is usual to merely evaluate a small number of extra data modalities in remote sensing.

Table 7. Evaluation results with missing, noisy and interfered DSM data on the hold-out test images of Vaihingen Dataset.

Modalities	OA	Surface	Building	Low-veg	Tree	Car	mF1
Baseline (IRRG+DSM)	0.913	0.930	0.952	0.843	0.900	0.908	0.907
(IRRG+missing-DSM)	0.908	0.926	0.949	0.839	0.897	0.903	0.903
(IRRG+random-noisy-data)	0.904	0.923	0.943	0.837	0.898	0.900	0.900
(IRRG+interfered-data)	0.899	0.905	0.943	0.836	0.892	0.902	0.896

6. Conclusions

We presented a novel pyramid attention and gated fusion method for multi-modality land cover and land use mapping in remote sensing. Our proposed pyramid attention fusion (PAF) module can effectively capture multi-level and cross-view attention maps to obtain rich and robust representations, that can further be flexibly harnessed as a key fusion bridge between multiple modalities using our developed gated fusion (GFU) algorithms. The GFU module can tune the noisy modalities and extract complementary features to improve the performance of our multimodal models. Built upon the PAF and GFU modules, our MultiModNet framework provides an end-to-end and lightweight multi-modal segmentation solution, which achieves the state-of-the-art performance and outperforms the strong baselines on two different representative remote sensing datasets. In addition, our methods easily generalize to more than two modalities for addressing more complicated problems in remote sensing.

Acknowledgements

The benchmark datasets: the Vaihingen dataset was provided by the International Society for Photogrammetry and Remote Sensing (ISPRS); the Agriculture-Vision dataset was provided by UIUC, IntelinAir and University of Oregon. This work was supported by the foundation of the Research Council of Norway under Grant 272399 and Grant 309439.

Disclosure statement

No potential conflict of interest was reported by the authors.

Funding

This work was supported by the foundation of Norges Forskningsråd under Grant 272399 and Grant 309439.

References

- Audebert, Nicolas, Bertrand Le Saux, and Sébastien Lefèvre. 2016. "Semantic segmentation of earth observation data using multimodal and multi-scale deep networks." In *Asian Conference on Computer Vision*, 180–196. Springer.
- Audebert, Nicolas, Bertrand Le Saux, and Sébastien Lefèvre. 2017. "Joint learning from earth observation and OpenStreetMap data to get faster better semantic maps." In *Proceedings of the IEEE Conference on Computer Vision and Pattern Recognition Workshops*, 67–75.
- Audebert, Nicolas, Bertrand Le Saux, and Sébastien Lefèvre. 2018. "Beyond RGB: Very high resolution urban remote sensing with multimodal deep networks." *ISPRS J. Photogramm. Remote Sensing* 140: 20–32.
- Audebert, Nicolas, Bertrand Le Saux, and Sébastien Lefèvre. 2019. "Deep learning for classification of hyperspectral data: A comparative review." *IEEE Geoscience and Remote Sensing Magazine* 7 (2): 159–173.
- Badrinarayanan, Vijay, Alex Kendall, and Roberto Cipolla. 2017. "SegNet: A Deep Convolutional Encoder-Decoder Architecture for Image Segmentation." *IEEE Transactions on Pattern Analysis and Machine Intelligence* 39 (12): 2481–2495.
- Bello, Olalekan Mumin, and Yusuf Adedoyin Aina. 2014. "Satellite remote sensing as a tool in disaster management and sustainable development: towards a synergistic approach." *Procedia-Social and Behavioral Sciences* 120: 365–373.
- Buslaev, Alexander, Vladimir I. Iglovikov, Eugene Khvedchenya, Alex Parinov, Mikhail Druzhinin, and Alexandr A. Kalinin. 2020. "Albumentations: Fast and Flexible Image Augmentations." *Information* 11 (2). <https://www.mdpi.com/2078-2489/11/2/125>.
- Chen, Liang-Chieh, George Papandreou, Iasonas Kokkinos, Kevin Murphy, and Alan L Yuille. 2018. "DeepLab: Semantic Image Segmentation with Deep Convolutional Nets, Atrous Convolution, and Fully Connected CRFs." *IEEE Trans. Pattern Anal. Mach. Intell.* 40 (4): 834–848.
- Chiu, Mang Tik, Xingqian Xu, Kai Wang, Jennifer Hobbs, Naira Hovakimyan, Thomas S. Huang, Honghui Shi, et al. 2020a. "The 1st Agriculture-Vision Challenge: Methods and Results." In *the IEEE/CVF Conference on Computer Vision and Pattern Recognition Workshops (CVPRW)*, 212–218.
- Chiu, Mang Tik, Xingqian Xu, Yunchao Wei, Zilong Huang, Alexander G. Schwing, Robert Brunner, Hrant Khachatrian, et al. 2020b. "Agriculture-Vision: A Large Aerial Image Database for Agricultural Pattern Analysis." In *the IEEE/CVF Conference on Computer Vision and Pattern Recognition (CVPR)*, June.
- Coupré, Camille, Clément Farabet, Laurent Najman, and Yann LeCun. 2013. "Indoor semantic segmentation using depth information." *arXiv preprint arXiv:1301.3572*.
- Dosovitskiy, Alexey, Lucas Beyer, Alexander Kolesnikov, Dirk Weissenborn, Xiaohua Zhai, Thomas Unterthiner, Mostafa Dehghani, et al. 2021. "An Image is Worth 16x16 Words: Transformers for Image Recognition at Scale." *ICLR*.
- Fan, Chao, Cheng Zhang, Alex Yahja, and Ali Mostafavi. 2021. "Disaster City Digital Twin:

- A vision for integrating artificial and human intelligence for disaster management.” *International Journal of Information Management* 56: 102049.
- Feng, Quanlong, Dehai Zhu, Jianyu Yang, and Baoguo Li. 2019. “Multisource hyperspectral and lidar data fusion for urban land-use mapping based on a modified two-branch convolutional neural network.” *ISPRS International Journal of Geo-Information* 8 (1): 28.
- Fu, J., J. Liu, H. Tian, Y. Li, Y. Bao, Z. Fang, and H. Lu. 2019. “Dual Attention Network for Scene Segmentation.” In *2019 IEEE/CVF Conference on Computer Vision and Pattern Recognition (CVPR)*, 3141–3149.
- Fu, Jun, Jing Liu, Haijie Tian, Yong Li, Yongjun Bao, Zhiwei Fang, and Hanqing Lu. 2019. “Dual attention network for scene segmentation.” In *Proceedings of the IEEE/CVF Conference on Computer Vision and Pattern Recognition*, 3146–3154.
- Ghosh, Arthita, Max Ehrlich, Sohil Shah, Larry Davis, and Rama Chellappa. 2018. “Stacked U-Nets for Ground Material Segmentation in Remote Sensing Imagery.” In *2018 IEEE/CVF Conference on Computer Vision and Pattern Recognition Workshops (CVPRW)*, 252–2524.
- Gómez-Chova, Luis, Devis Tuia, Gabriele Moser, and Gustau Camps-Valls. 2015. “Multimodal classification of remote sensing images: A review and future directions.” *Proceedings of the IEEE* 103 (9): 1560–1584.
- Hazirbas, Caner, Lingni Ma, Csaba Domokos, and Daniel Cremers. 2016. “Fusenet: Incorporating depth into semantic segmentation via fusion-based cnn architecture.” In *Asian Conference on Computer Vision*, 213–228. Springer.
- Hong, Danfeng, Lianru Gao, Naoto Yokoya, Jing Yao, Jocelyn Chanussot, Qian Du, and Bing Zhang. 2020. “More diverse means better: Multimodal deep learning meets remote-sensing imagery classification.” *IEEE Transactions on Geoscience and Remote Sensing*.
- Howard, Andrew, Mark Sandler, Grace Chu, Liang-Chieh Chen, Bo Chen, Mingxing Tan, Weijun Wang, et al. 2019. “Searching for mobilenetv3.” In *Proceedings of the IEEE/CVF International Conference on Computer Vision*, 1314–1324.
- Hu, Jie, Li Shen, and Gang Sun. 2018. “Squeeze-and-excitation networks.” In *Proceedings of the IEEE Conference on Computer Vision and Pattern Recognition*, 7132–7141.
- Jiang, Jie, Chengjin Lyu, Siying Liu, Y. He, and Xuetao Hao. 2020. “RWSNet: a semantic segmentation network based on SegNet combined with random walk for remote sensing.” *International Journal of Remote Sensing* 41: 487 – 505.
- Kampffmeyer, Michael, Arnt-Borre Salberg, and Robert Jenssen. 2016. “Semantic segmentation of small objects and modeling of uncertainty in urban remote sensing images using deep convolutional neural networks.” In *Proceedings of the IEEE Conference on Computer Vision and Pattern Recognition Workshops*, 1–9.
- Kampffmeyer, Michael, Arnt-Børre Salberg, and Robert Jenssen. 2018. “Urban Land Cover Classification With Missing Data Modalities Using Deep Convolutional Neural Networks.” *IEEE Journal of Selected Topics in Applied Earth Observations and Remote Sensing* 11 (6): 1758–1768.
- Kingma, Diederik P., and Jimmy Ba. 2014. “Adam: A Method for Stochastic Optimization.” *CoRR* abs/1412.6980. <http://arxiv.org/abs/1412.6980>.
- Kipf, Thomas N, and Max Welling. 2016. “Semi-supervised classification with graph convolutional networks.” *arXiv preprint arXiv:1609.02907*.
- Li, Xiao, Lin Lei, Yuli Sun, Ming Li, and Gangyao Kuang. 2020. “Multimodal bilinear fusion network with second-order attention-based channel selection for land cover classification.” *IEEE Journal of Selected Topics in Applied Earth Observations and Remote Sensing* 13: 1011–1026.
- Lin, Guosheng, Chunhua Shen, Anton Van Den Hengel, and Ian Reid. 2016. “Efficient piecewise training of deep structured models for semantic segmentation.” In *Proceedings of the IEEE Conference on Computer Vision and Pattern Recognition*, 3194–3203.
- Lin, Tsung-Yi, Piotr Dollár, Ross Girshick, Kaiming He, Bharath Hariharan, and Serge Belongie. 2017. “Feature pyramid networks for object detection.” In *Proceedings of the IEEE Conference on Computer Vision and Pattern Recognition*, 2117–2125.
- Liu, Q., M. Kampffmeyer, R. Jenssen, and A. B. Salberg. 2020. “Dense Dilated Convolutions’

- Merging Network for Land Cover Classification.” *IEEE Transactions on Geoscience and Remote Sensing* 58 (9): 6309–6320.
- Liu, Qinghui, Michael Kampffmeyer, Robert Jenssen, and Arnt-Børre Salberg. 2020a. “Self-Constructing Graph Convolutional Networks for Semantic Labeling.” In *Proceedings of IGARSS 2020 - 2020 IEEE International Geoscience and Remote Sensing Symposium*, .
- Liu, Qinghui, Michael C. Kampffmeyer, Robert Jenssen, and Arnt-Børre Salberg. 2020b. “Multi-View Self-Constructing Graph Convolutional Networks With Adaptive Class Weighting Loss for Semantic Segmentation.” In *the IEEE/CVF Conference on Computer Vision and Pattern Recognition (CVPR) Workshops*, June.
- Liu, Yansong, Sankaranarayanan Piramanayagam, Sildomar T Monteiro, and Eli Saber. 2019. “Semantic segmentation of multisensor remote sensing imagery with deep ConvNets and higher-order conditional random fields.” *Journal of Applied Remote Sensing* 13 (1): 016501.
- Long, Jonathan, Evan Shelhamer, and Trevor Darrell. 2015. “Fully Convolutional Networks for Semantic Segmentation.” In *Proceedings of the IEEE Conference on Computer Vision and Pattern Recognition*, 3431–3440.
- Maggiori, Emmanuel, Yuliya Tarabalka, Guillaume Charpiat, and Pierre Alliez. 2017. “Can semantic labeling methods generalize to any city? the inria aerial image labeling benchmark.” In *2017 IEEE International Geoscience and Remote Sensing Symposium (IGARSS)*, 3226–3229. IEEE.
- Marmanis, Dimitrios, Konrad Schindler, Jan Dirk Wegner, Silvano Galliani, Mihai Datcu, and Uwe Stilla. 2016. “Classification With an Edge: Improving Semantic Image Segmentation with Boundary Detection.” *CoRR* abs/1612.01337. <http://arxiv.org/abs/1612.01337>.
- Mohla, Satyam, Shivam Pande, Biplab Banerjee, and Subhasis Chaudhuri. 2020. “FusAtNet: Dual Attention based SpectroSpatial Multimodal Fusion Network for Hyperspectral and LiDAR Classification.” In *2020 IEEE/CVF Conference on Computer Vision and Pattern Recognition Workshops (CVPRW)*, 416–425.
- Mou, Lichao, and Xiao Xiang Zhu. 2019. “Learning to pay attention on spectral domain: A spectral attention module-based convolutional network for hyperspectral image classification.” *IEEE Transactions on Geoscience and Remote Sensing* 58 (1): 110–122.
- Noor, Norzailawati Mohd, Alias Abdullah, and Mazlan Hashim. 2018. “Remote sensing UAV/drones and its applications for urban areas: a review.” In *IOP conference series: Earth and environmental science*, Vol. 169, 012003. IOP Publishing.
- Paisitkriangkrai, Sakrapee, Jamie Sherrah, Pranam Janney, Van-Den Hengel, et al. 2015. “Effective semantic pixel labelling with convolutional networks and conditional random fields.” In *Proceedings of the IEEE Conference on Computer Vision and Pattern Recognition Workshops*, 36–43.
- Pashaei, Mohammad, Hamid Kamangir, Michael J Starek, and Philippe Tissot. 2020. “Review and evaluation of deep learning architectures for efficient land cover mapping with UAS hyper-spatial imagery: A case study over a wetland.” *Remote Sensing* 12 (6): 959.
- Ronneberger, Olaf, Philipp Fischer, and Thomas Brox. 2015. “U-Net: Convolutional networks for biomedical image segmentation.” In *International Conference on Medical Image Computing and Computer-Assisted Intervention*, 234–241. Springer.
- Rottensteiner, Franz, Gunho Sohn, Jaewook Jung, Markus Gerke, Caroline Baillard, Sebastien Benitez, and Uwe Breitkopf. 2012. “The ISPRS benchmark on urban object classification and 3D building reconstruction.” *ISPRS Annals of the Photogrammetry, Remote Sensing and Spatial Information Sciences I-3 (2012)*, Nr. 1 1 (1): 293–298.
- Salberg, Arnt-Børre. 2011. “Land Cover Classification of Cloud-Contaminated Multitemporal High-Resolution Images.” *IEEE Transactions on Geoscience and Remote Sensing* 49 (1): 377–387.
- Salberg, Arnt-Børre, Øystein Rudjord, and Anne H. Schistad Solberg. 2014. “Oil Spill Detection in Hybrid-Polarimetric SAR Images.” *IEEE Transactions on Geoscience and Remote Sensing* 52 (10): 6521–6533.
- Sherrah, Jamie. 2016. “Fully Convolutional Networks for Dense Semantic Labelling of High-Resolution Aerial Imagery.” *CoRR* abs/1606.02585. <http://arxiv.org/abs/1606.02585>.

- Vaswani, Ashish, Noam Shazeer, Niki Parmar, Jakob Uszkoreit, Llion Jones, Aidan N Gomez, Łukasz Kaiser, and Illia Polosukhin. 2017. “Attention is All you Need.” In *Advances in Neural Information Processing Systems 30*, edited by I. Guyon, U. V. Luxburg, S. Bengio, H. Wallach, R. Fergus, S. Vishwanathan, and R. Garnett, 5998–6008. Curran Associates, Inc. <http://papers.nips.cc/paper/7181-attention-is-all-you-need.pdf>.
- Wang, Hongzhen, Ying Wang, Qian Zhang, Shiming Xiang, and Chunhong Pan. 2017. “Gated convolutional neural network for semantic segmentation in high-resolution images.” *Remote Sensing* 9 (5): 446.
- Xu, Xiaodong, Wei Li, Qiong Ran, Qian Du, Lianru Gao, and Bing Zhang. 2017. “Multisource remote sensing data classification based on convolutional neural network.” *IEEE Transactions on Geoscience and Remote Sensing* 56 (2): 937–949.
- Xu, Yonghao, Bo Du, and Liangpei Zhang. 2018. “Multi-Source Remote Sensing Data Classification via Fully Convolutional Networks and Post-Classification Processing.” In *IGARSS 2018 - 2018 IEEE International Geoscience and Remote Sensing Symposium*, 3852–3855.
- Xu, Yonghao, Bo Du, Liangpei Zhang, Daniele Cerra, Miguel Pato, Emiliano Carmona, Saurabh Prasad, Naoto Yokoya, Ronny Hänsch, and Bertrand Le Saux. 2019. “Advanced Multi-Sensor Optical Remote Sensing for Urban Land Use and Land Cover Classification: Outcome of the 2018 IEEE GRSS Data Fusion Contest.” *IEEE Journal of Selected Topics in Applied Earth Observations and Remote Sensing* 12 (6): 1709–1724.
- Yuan, Yuhui, Xilin Chen, and Jingdong Wang. 2020. “Object-Contextual Representations for Semantic Segmentation.” In *Proceedings of the European Conference on Computer Vision (ECCV)*, 173–190.
- Zhao, Hengshuang, Jianping Shi, Xiaojuan Qi, Xiaogang Wang, and Jiaya Jia. 2017. “Pyramid Scene Parsing Network.” In *2017 IEEE Conference on Computer Vision and Pattern Recognition (CVPR)*, 6230–6239.